OUKA
Osaka University Knowledge Archive

Title	Molecular dynamics simulation of silicon and silicon dioxide etching by energetic halogen beams
Author(s)	Ohta, H.; Hamaguchi, S.
Citation	Journal of Vacuum Science and Technology, Part A: Vacuum, Surfaces and Films. 19(5) p.2373-p.2381
Issue Date	2001-09
oaire:version	VoR
URL	https://hdl.handle.net/11094/78493
rights	This article may be downloaded for personal use only. Any other use requires prior permission of the author and AIP Publishing. This article appeared in Journal of Vacuum Science & Technology A 19, 2373 (2001) and may be found at https://doi.org/10.1116/1.1385906.
Note	

Osaka University Knowledge Archive : OUKA

https://ir.library.osaka-u.ac.jp/

Osaka University

JVST A
Journal of Vacuum Science & Technology A

Molecular dynamics simulation of silicon and silicon dioxide etching by energetic halogen beams

Cite as: Journal of Vacuum Science & Technology A **19**, 2373 (2001); https://doi.org/10.1116/1.1385906
Submitted: 20 December 2000 . Accepted: 21 May 2001 . Published Online: 13 September 2001

H. Ohta, and S. Hamaguchi


View Online

Export Citation

ARTICLES YOU MAY BE INTERESTED IN

Overview of atomic layer etching in the semiconductor industry
Journal of Vacuum Science & Technology A **33**, 020802 (2015); https://doi.org/10.1116/1.4913379

Classical interatomic potentials for Si–O–F and Si–O–Cl systems
The Journal of Chemical Physics **115**, 6679 (2001); https://doi.org/10.1063/1.1400789

Molecular dynamics simulations of Si etching by energetic CF_3^+
Journal of Applied Physics **86**, 5938 (1999); https://doi.org/10.1063/1.371637

© 2001 American Vacuum Society.

Molecular dynamics simulation of silicon and silicon dioxide etching by energetic halogen beams

H. Ohta[a] and S. Hamaguchi[b]
Department of Fundamental Energy Science, Kyoto University, Gokasho, Uji, Kyoto 611-0011, Japan

(Received 20 December 2000; accepted 21 May 2001)

Molecular dynamics simulations of silicon (Si) and silicon dioxide (SiO_2) etching by energetic halogen (fluorine or chlorine) atoms in the energy range of 50–150 eV are performed using new sets of interatomic potentials for Si–O–F and Si–O–Cl systems. Etch rates and selectivities obtained from numerical simulations are compared with available experimental data. Etching mechanisms in the atomic scale, especially the difference between chlorine and fluorine direct ion etching characteristics, are discussed on the basis of the simulation results. © *2001 American Vacuum Society.* [DOI: 10.1116/1.1385906]

I. INTRODUCTION

It is of great importance in semiconductor surface processing to understand plasma–surface interactions in the atomic scale and to create a database for fundamental surface reactions. Such understandings can facilitate further progress in process technologies for submicron structures with nanoscale accuracy. Unfortunately, due to the difficulty of precise *in situ* measurements of various surface reactions, our knowledge of fundamental reaction dynamics on the surface is currently limited. However, atomic-scale molecular dynamics (MD) simulations may be used to compensate for the lack of some experimental data and give insight into the mechanisms of fundamental surface reactions. One of the advantages of MD simulations is that one can perform controlled ''experiments'' under ideal conditions in order to elucidate particular aspects of reaction dynamics. Furthermore, a systematic parameter survey by MD simulations can be used to create a database for fundamental reactions cost effectively if the simulation data are critically checked against relevant experimental data.

One of the most essential and hardest tasks regarding classical MD simulations is the selection and/or construction of interatomic potentials representing the physical systems. The classical interatomic potentials for Si–F and Si–Cl systems were developed by Stillinger and Weber[1–4] and by Feil *et al.*,[5] respectively. Using these potentials, several authors performed numerical simulations of silicon etching by Cl or F.[6–12] Improvement of these classical potentials for Si–F and Si–Cl systems were also attempted. Weakliem *et al.* and Carter *et al.* modified the original Stillinger–Weber (SW) potentials by fitting the potential functions to data obtained from the first-principle quantum mechanical calculations and, using the modified potentials, performed more realistic simulations for fluorine adsorption on Si surfaces.[13–15] Hanson *et al.* also modified the SW potentials for Si–Cl systems by adding embedded potential and four-body terms. Using the new potentials, they calculated Si etch rates by Cl, showing the newly obtained etch rates are in better agreement with experimental data than those obtained based on the original potentials.[16,17]

To the best of our knowledge, however, MD simulations of silicon dioxide (SiO_2) etching by halogen atoms had not been performed previously despite its importance as, e.g., hard masks for Si etching processes. This is probably because classical interatomic potentials for Si–O–F or Si–O–Cl systems were not previously available. Using previously available potentials, a few authors studied Ar sputtering of SiO_2.[18–20] In this article, we present MD simulation results for SiO_2 etching by halogen atoms. For this purpose, we have constructed new sets of interatomic potentials for Si–O–F and Si–O–Cl systems based on data obtained from the first-principle quantum mechanical calculations and have completely rewritten our previous MD simulation code[21] to incorporate multibody potentials.

The goal of this work is to understand details of silicon and silicon dioxide etching characteristics by energetic halogens. In this work, we focus on direct ion etching, where all reactive halogen atoms are directed to the surface with considerable energies. Therefore, MD simulations presented here correspond to ion beam etching, rather than reactive ion etching (RIE), where low-energy background neutral atoms covering the surface play important roles in surface reactions. Etch rates and selectivities (the ratios of silicon to oxide etch rates), which affect micron- or submicron-scale feature profiles, are obtained from numerical simulations. We also discuss etching mechanisms in the atomic scale based on MD simulation results, especially focusing on selectivities and different characteristics between chlorine and fluorine direct ion etching.

II. MOLECULAR DYNAMICS SIMULATION

To emulate the surface reactions just discussed by numerical simulations, we consider the following model. A single atom (either halogen or noble gas) is directed to the target with the normal incident angle. In the present work, the target is either Si or SiO_2. In ion beam experiments, energetic ions impinging on the surface are expected to be neutralized right before interacting with the target surface due to an Auger emission process. Therefore, in our simula-

[a]Electronic mail: ohta@center.iae.kyoto-u.ac.jp
[b]Electronic mail: hamaguch@energy.kyoto-u.ac.jp

TABLE I. Binding energies and bond lengths are shown.

	Binding energy		
	(eV)	(kcal/mol)	Bond length (Å)
Si–Si	2.17	50.0	2.35
Si–O	4.14	95.4	1.61
Si–Cl	3.96	91.2	2.06
Cl–Cl	2.47	56.9	1.96
Cl–O	2.09	48.2	1.62
Si–F	5.72	132	1.60
F–F	1.66	38.3	1.43
F–O	2.18	50.2	1.36

tions, only charge–neutral atoms are used as impinging species. It is also assumed that the target surface is kept charge neutral during the process. The energy range of impinging atoms employed in our numerical experiments is 50–150 eV and the target surface is initially kept at 300 K. For the sake of simplicity, polyatomic species are not used for impinging particles here.

To represent the aforementioned model numerically, we use classical molecular dynamics (MD) simulation. The interatomic potential functions are selected to reproduce binding energies, valences for covalent binding, and appropriate structures of the materials with good accuracy. As in earlier studies,[5–10,12] we employ the SW potentials[1–5] to represent interactions among Si and halogens (either F or Cl). To model systems containing only Si and O, we use the potential functions obtained by Watanabe *et al.*[22] In oxide etching simulations by halogens, however, we need to deal with ternary interactions among Si, O, and F (or Cl). To the best of our knowledge, there had been no available classical potential functions to represent such interactions, so we have constructed SW type interatomic potentials for Si–O–F and Si–O–Cl systems, which are summarized in Appendix A. The potential functions were determined by nonlinearly fitting appropriate functional forms to potential energy data obtained from *ab initio* quantum mechanical calculations. The obtained potential functions are compatible with the SW potentials for Si and halogen systems as well as the Si–O system potentials of Watanabe *et al.*[22] The derivation of the interatomic potentials for Si–O–F and Si–O–Cl systems will be published elsewhere.[23] The interatomic potentials between Ar and other atoms are modeled by the repulsive Moliére pair potentials.[24] Table I shows the energies and lengths of some representative bonds derived from the potential functions used in our simulations.

The equations of motion based on the interparticle potentials just mentioned are solved numerically with variable time steps determined from the velocity of the fastest particle.[25] The typical time step in our simulation is 0.2–0.5 fs which is small enough to guarantee good conservation of total energies of isolated systems. As shown in Fig. 1, the target material is placed in a simulation cell with periodic boundary conditions imposed in the horizontal directions. The atoms in the bottom layer are rigidly fixed to prevent the drift of the whole cell by the particle bombardment. The

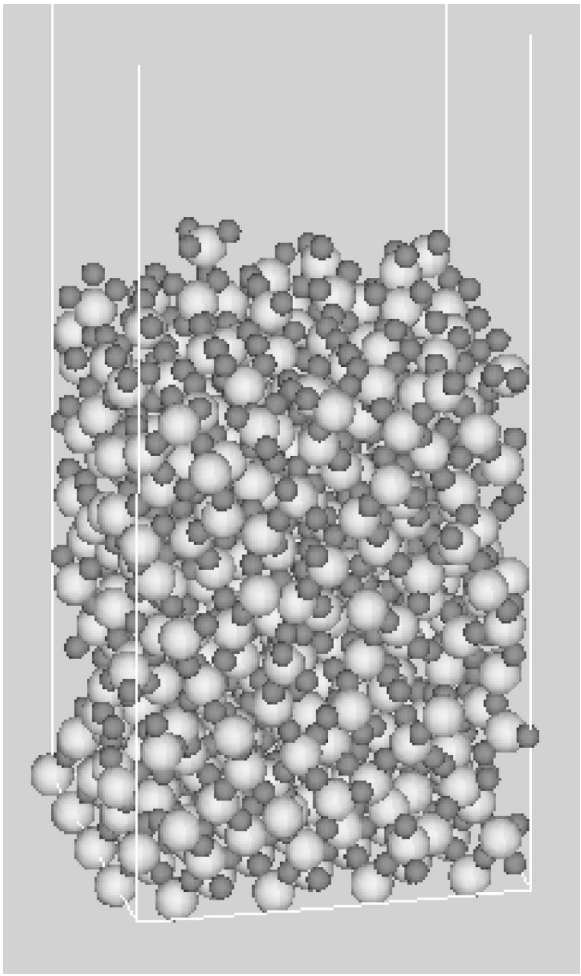

FIG. 1. The initial structure of a SiO_2 target is shown. The simulation cell contains 384 silicon atoms (large white spheres) and 768 oxygen atoms (small gray spheres).

initial structures of the target are the diamond lattice for Si [with the top surface being (100)] and a relaxed amorphous structure initially arranged as the pseudo β cristobalite for SiO_2. Figure 1 shows an example of such amorphous structures of the oxide target. Physical quantities such as sputtering yields are measured only after surface conditions reach a ''steady state'' by sufficient particle bombardment. The simulation surface is a square of side length 21.7 Å (the area is 472 $Å^2$) with a monolayer initially including 32 Si atoms for the silicon target and 32 Si and 64 O atoms for the oxide target. We have also increased the simulation area up to 737 $(=27.2^2)$ $Å^2$ for some simulation runs and confirmed that the simulation surface size of 472 $(=21.7^2)$ $Å^2$ is sufficiently large to guarantee that obtained sputtering data are essentially independent of the area size under sputtering conditions employed in this work. Initially, the target materials are composed of 16 monolayers for Si (i.e., 512 Si atoms) and 12 monolayers for oxide (i.e., 384 Si atoms and 768 O atoms, totaling 1152 atoms), the depths of which are 21 Å for Si and 32 Å for oxide. Energetic particles are injected from randomly chosen locations just above the target in the direction normal to the surface. It is sometimes more convenient

to measure the dose of impinging particles in units of monolayer (ML), with 1 ML corresponding to 32 impinging particles in both Si and oxide cases in our simulation. The bombardment process by a single energetic particle is then repeated about 1000 times (i.e., about 31 ML) to increase statistics for the measurement of macroscopic parameters such as sputtering yields.

Most transient etching processes such as breaking and reformation of bonds by particle bombardment typically occur within a picosecond. On the other hand, under ordinary plasma processing conditions, the interval between two successive ion injection into such a small simulation surface area is of order 1 μs. Therefore, each ion bombardment may be considered as an independent process. To simulate such independent processes efficiently, for the first 0.7 ps after an energetic particle hits the surface, the motion of all particles are solved numerically except for those on the rigidly fixed bottom layer. Then, we apply artificial cooling to all the particles for 0.3 ps, using Berendsen's heat removal scheme[26] with a coupling constant of $2.0\times10^{-14}\,\mathrm{s}^{-1}$. At the end of the cooling process, a new energetic particle is directed again to the surface and the whole simulation cycle is repeated. Etching products—defined as (clusters of) atoms that are isolated from the surface and have momentum in the direction away from surface—are automatically detected and recorded during simulations and then removed from the simulation cell at the end of each simulation cycle. To avoid depletion of simulation particles, a new layer of atoms is automatically added to the simulation cell from the bottom occasionally.

The surface conditions greatly influence sputtering yields. One of the critical issues pertaining to such MD simulations is how to obtain the ''typical'' surface in an etching process. As we have mentioned earlier, we start from a clean target surface and continue to bombard the surface until we observe the surface roughness and properties of the halogenated layer (in the case of halogen bombardment) reach a steady state. We measure physical quantities such as etch rates only after surface conditions reach such a steady state, which is typically after bombardment of about 10 ML atoms.

The question then arises whether the surface conditions in such steady states actually represent the typical surface conditions. It is not easy to answer this question since we artificially cool the surface 0.7 ps after each ion impingement, which quenches the surface morphology quite rapidly. Such artificial cooling processes are necessary in MD simulations to prevent the simulation system from being unrealistically heated up. In a real system, however, the energy deposited in a small region near the surface dissipates by phonon propagation and thermal diffusion. These dissipation processes take place in a much longer time scale than the artificial cooling process, which lasts only for 0.3 ps in our simulation. Of course, it is not practical to simulate such long-time dissipation processes directly by MD simulations. Therefore steady-state surfaces obtained in our MD simulations may be somewhat rougher than the actual surfaces during etching processes.

In etching simulations, we sometimes observe large clusters of atoms (i.e., molecules or radicals) are desorbed from the surface. Although such events are not so frequent, even a small number of such clusters can significantly increase sputtering yields since the number of atoms constituting such clusters can be very large. Desorption of large molecules and clusters may indeed occur in actual etching processes. However, we think it is much less frequent than we observe in our numerical simulations since, as we have noted, surfaces obtained in MD simulations may be rougher than the actual surfaces, i.e., surface atoms in MD simulations may be less firmly bonded. In what follows, therefore, we define the sputtering yield Y of Si from the Si or SiO_2 surface as the number of Si atoms desorbed in the form of $SiCl_x$ or $SiCl_xO_y$ (x and $y\geqslant 0$) par Cl impact (SiF_x or SiF_xO_y par F impact). In other words, we ignore desorbed clusters containing more than two Si atoms in evaluating the sputtering yield. In this sense, yield Y defined here gives a lower bound of the actual sputtering yield. However, as we have observed in our simulations and as also demonstrated in earlier Si etching simulations by Hanson *et al.*,[16,17] desorbed products are predominantly clusters containing single Si atoms. Therefore, sputtering yield Y thus defined is expected to be sufficiently close to the actual sputtering yield.

III. RESULTS AND DISCUSSION

A. Si etching

Molecular dynamics simulations for halogen/silicon etching have been performed extensively by many authors[5–10,12,16,17] using various potential forms and different surface conditions. In order to evaluate Si and SiO_2 etch rates on the same footing so that we can obtain the selectivity self-consistently, we have also performed MD simulations for Si etching with the SW potentials. Table II lists Si sputtering yields for silicon and oxide targets obtained from our MD simulations. Sputtering yield Y is defined in the preceding section. For comparison, we also list yield Y_2, which is defined as the number of Si atoms desorbed in the form of clusters containing up to 2 Si atoms (e.g., clusters such as Si_mCl_x or $Si_mCl_xO_y$ with $m=1$ and 2 for Cl impact) par impact atom. Clearly, $Y\leqslant Y_2$. As we discussed previously, however, Y_2 may overestimate the actual sputtering yield. The sputtering yields due to pure physical sputtering, i.e., sputtering by Ar atoms, are also listed in Table II. Large sputtering yields for halogens are generally attributed to chemical effects, as we shall discuss momentarily.

The sputtering yields presented in this work are obtained by averaging the yield values from the 321st to 960th impact (11–30 ML runs). The surface may be considered to have reached the steady state if (a) the depth of halogenated layer, (b) fractions of each element in the halogenated layer, and (c) the number of halogens (i.e., halogen content) in the simulation cell are all observed to become almost constant. This typically occurs after 10 ML atomic bombardment in our MD simulations, as mentioned before. The values of (a)–(c) mentioned in steady states averaged over 11–30 ML simulation cycles are given in Table III. Here, the depth of a

TABLE II. Silicon sputtering yields obtained from MD simulations under various etching conditions are shown. Sputtering yield Y denotes the number of Si atoms desorbed from the surface in the form of SiC_x or SiC_xO_y (SiF_x or SiF_xO_y) per impact atom. For the definition of Y_2, see the main text. The yields are averages over 321–960 (11–30 ML) impact runs.

Target/Beam	Y	Y_2
Si/Cl 20 eV	0.10	0.13
Si/Cl 30 eV	0.16	0.19
Si/Cl 50 eV	0.26	0.31
Si/Cl 100 eV	0.46	0.57
Si/Cl 150 eV	0.67	0.84
Si/F 50 eV	0.42	0.47
Si/F 100 eV	0.51	0.60
Si/F 150 eV	0.62	0.75
Si/Ar 50 eV	0.011	0.011
Si/Ar 100 eV	0.084	0.088
Si/Ar 150 eV	0.15	0.16
SiO_2/Cl 50 eV	0.020	0.023
SiO_2/Cl 100 eV	0.11	0.13
SiO_2/Cl 150 eV	0.15	0.21
SiO_2/F 50 eV	0.12	0.16
SiO_2/F 100 eV	0.20	0.25
SiO_2/F 150 eV	0.22	0.30
SiO_2/Ar 50 eV	0.0031	0.0031
SiO_2/Ar 100 eV	0.039	0.045
SiO_2/Ar 150 eV	0.067	0.092

halogenated layer is defined, for the sake of simplicity, as the distance between the most deeply penetrated halogen atom and the atom of any kind located in the highest position of the target.

Figure 2 plots the sputtering yields (Y in Table II) for Si targets. Here ○, □, and △ indicate the Si sputtering yields by Cl, F, and Ar impact, respectively. We note that these values are in good agreement with earlier simulation results given in Refs. 7, 9, 16, and 17. The fitting curves shown in Fig. 2 are based on the function (Ref. 27) $Y=A(E^{1/2}-B)$, where E is the incident energy in eV and the obtained fitting

TABLE III. Halogenated layer depths, fractions of elements in the halogenated layers, and halogen contents in the simulation cell obtained from MD simulations. The values are averages over 321–960 (11–30 ML) impact runs.

		Fraction of Elements			
Target/Beam	Depth (Å)	Si	Cl or F	O	Cl or F content
Si/Cl 20 eV	13	0.65	0.35	···	53 (1.7 ML)
Si/Cl 30 eV	15	0.67	0.33	···	56 (1.7 ML)
Si/Cl 50 eV	23	0.82	0.18	···	62 (1.9 ML)
Si/Cl 100 eV	27	0.83	0.17	···	60 (1.9 ML)
Si/Cl 150 eV	32	0.84	0.16	···	68 (2.1 ML)
Si/F 50 eV	31	0.75	0.25	···	107 (3.4 ML)
Si/F 100 eV	43	0.74	0.26	···	155 (4.8 ML)
Si/F 150 eV	49	0.80	0.20	···	141 (4.4 ML)
SiO_2/Cl 50 eV	13	0.27	0.23	0.50	59 (1.8 ML)
SiO_2/Cl 100 eV	28	0.29	0.16	0.55	92 (2.9 ML)
SiO_2/Cl 150 eV	27	0.30	0.15	0.55	69 (2.2 ML)
SiO_2/F 50 eV	23	0.26	0.22	0.52	114 (3.6 ML)
SiO_2/F 100 eV	29	0.28	0.20	0.52	107 (3.3 ML)
SiO_2/F 150 eV	38	0.30	0.18	0.53	125 (3.9 ML)

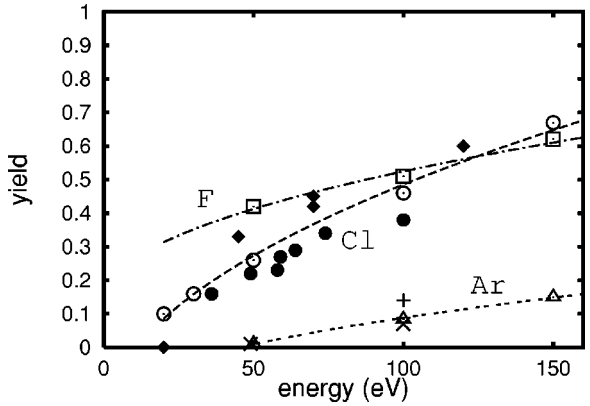

FIG. 2. Silicon sputtering yields (given by Y in Table II) of the silicon target for Cl (○), F (□), and Ar (△) beam etching are shown. Experimental data for Cl^+ beam etching by Chang and Sawin (Ref. 28) and chlorine plasma etching by Holber *et al.* (Ref. 29) are denoted by ●'s and ◆'s respectively. Experimental data for Si sputtering by Ar beams are denoted by ×'s [obtained by Chang *et al.* (Ref. 30)] and +'s [obtained by Tachi and Okudaira (Ref. 31)]. The dashed, dotted–dashed, and dotted curves are yield fitting curves for Cl, F, and Ar beam etching processes, respectively, as given in the main text.

parameters are $A=0.0382$ and $B=-3.73$ for F, $A=0.0723$ and $B=3.29$ for Cl, and $A=0.0268$ and $B=6.72$ for Ar. If $B\geqslant 0$, the threshold energy is given by $E_{th}=B^2$ and we have obtained $E_{th}\simeq 11$ eV for Cl and $E_{th}\simeq 45$ eV for Ar.

For comparison, experimentally obtained Si yields are also plotted in Fig. 2: ●'s denote data from Cl^+ beam etching by Chang and Sawin[28] and ◆'s from chlorine plasma etching by Holber and Forster.[29] Experimental data of Si yields by Ar beam etching are denoted by ×'s (obtained by Chang *et al.*)[30] and +'s (obtained by Tachi and Okudaira.)[31] Our simulation results are shown to be in good agreement with the experimental data. The simulation results show that sputtering yields by F impact are larger than those by Cl impact in the energy range less than around 120 eV and are smaller in the higher-energy range. This is consistent with experimental observations by Tachi and Okudaira.[31] Such a crossover of sputtering yields may be explained in the following manner.

As the Si–F and Si–Cl bond lengths given in Table I indicate, the size of a fluorine atom is much smaller than that of a chlorine atom. Therefore, with the same impact energy, fluorine atoms can penetrate the Si target more deeply than chlorine atoms. In addition, the Si–F binding energy is higher than the Si–Cl binding energy, so F atoms are more easily bound by Si atoms once they are in the Si target. This is consistent with the *ab initio* calculation results by Seel and Bagus,[32] which have shown that the penetration energy barrier into Si clusters is significantly higher for Cl than that for F. These effects result in deeper halogenated layers and higher halogen concentrations in the layers for sputtering by F atoms, as shown in Table III. Note that, in halogenated layers, many Si bonds are terminated by halogen atoms in such a way that Si atoms are more weakly bound with other Si atoms and therefore more likely to be removed by atomic impact than those in the original Si crystal. Sputtering en-

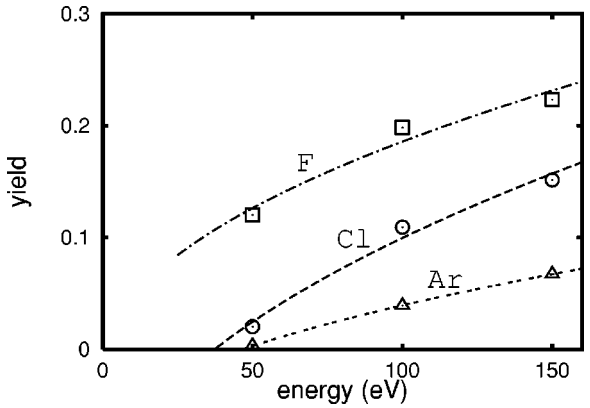

FIG. 3. Silicon sputtering yields (given by Y in Table II) of the oxide (SiO_2) target for Cl (○), F (□), and Ar (△) beam etching are shown. The dashed, dotted–dashed, and dotted curves are yield fitting curves for Cl, F, and Ar beam etching processes, respectively, as given in the main text.

hanced by chemical reactions are called chemical sputtering. In the low-energy regime, impinging F atoms have higher sputtering yields than Cl atoms since F atoms can form more effective halogenated layers.

In the higher energy regime, both Cl and F atoms can halogenate the target surface sufficiently. However, as shown in Table III, the depth of the fluorinated layer is much larger than the chlorinated layer for the same impact energy. In other words, with the same impact energy, an impinging F atom travels longer in the deep fluorinated layer before releasing its kinetic energy completely whereas an impinging Cl atom releases most of its kinetic energy in the shallow chlorinated layer. Therefore, the incoming kinetic energy is more efficiently used to break surface bonds in the case of Cl sputtering, which results in higher sputtering yields for Cl in the high-energy regime.

B. SiO_2 etching

The sputtering yields (Y in Table II) for oxide targets are plotted in Fig. 3. Here ○, □, and △ denote Si sputtering yields by Cl, F, and Ar impact, respectively. As in Fig. 2, the functional form $Y=A(E^{1/2}-B)$ was used to fit the yield data, where the fitting parameters are $A=0.0203$ and $B=0.850$ for F, $A=0.0256$ and $B=6.11$ for Cl, and $A=0.0124$ and $B=6.83$ for Ar. The estimated threshold energy is $E_{th}(=B^2)\simeq 37$ eV for Cl and $E_{th}\simeq 47$ eV for Ar.

The Si sputtering yields of oxide by Ar impact obtained from our simulations agree with earlier MD simulation results based on different interatomic potentials.[18] Our estimate of the oxide etching threshold energy $E_{th}\simeq 47$ eV is in good agreement with that by Holber and Forster.[29] Oostra *et al.* have also confirmed experimentally that oxide etching does not occur for Ar^+ impact with normal incidence at about 50 eV.[33] Note that sputtering yields by Ar beams for SiO_2 is much smaller than that for Si since the Si–O binding energy is significantly higher than the Si–Si binding energy.

Since in the bulk of SiO_2 each silicon atom has four Si–O covalent bonds whereas each oxygen atom has only two, oxygen atoms can be more easily removed by physical sputtering than silicon atoms. In the early stage of simulation where a clean SiO_2 target surface is subject to the atomic bombardment, we observe that more oxygen atoms are removed from the surface than Si atoms. A similar phenomenon was observed in earlier MD simulations for Ar sputtering of oxide targets.[19,20] In the case of halogen sputtering, the remaining excessive silicon atoms on the surface are then removed efficiently by the combination of physical and chemical sputtering, as in the case of silicon etching by halogens. In steady states, physical sputtering of oxygen atoms and physical/chemical sputtering of Si atoms are balanced.

The fact that oxygen atoms are more easily removed from

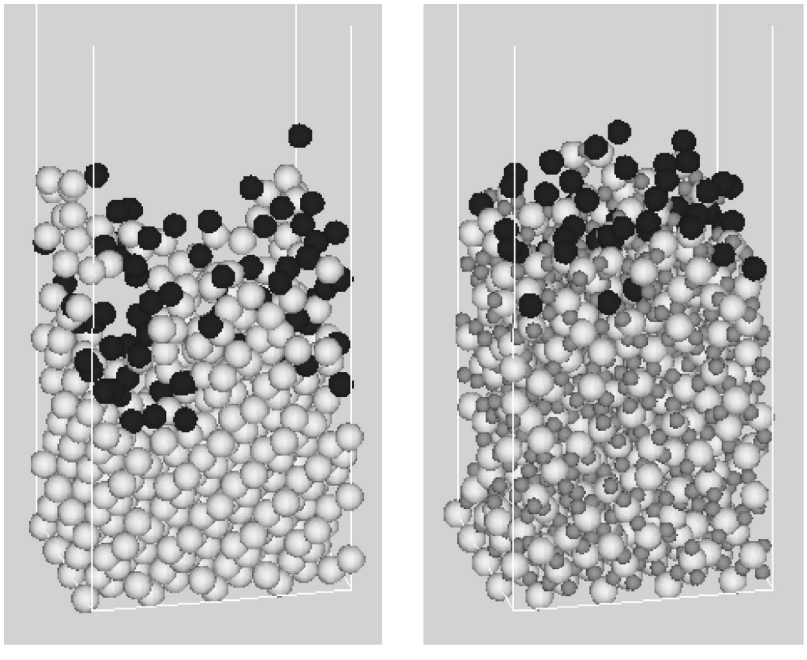

FIG. 4. Typical surface structures during 50 eV Cl beam etching; the Si (a) and SiO_2 (b) targets are shown. Large white spheres are Si atoms, small gray spheres are O atoms, and large black spheres are Cl atoms.

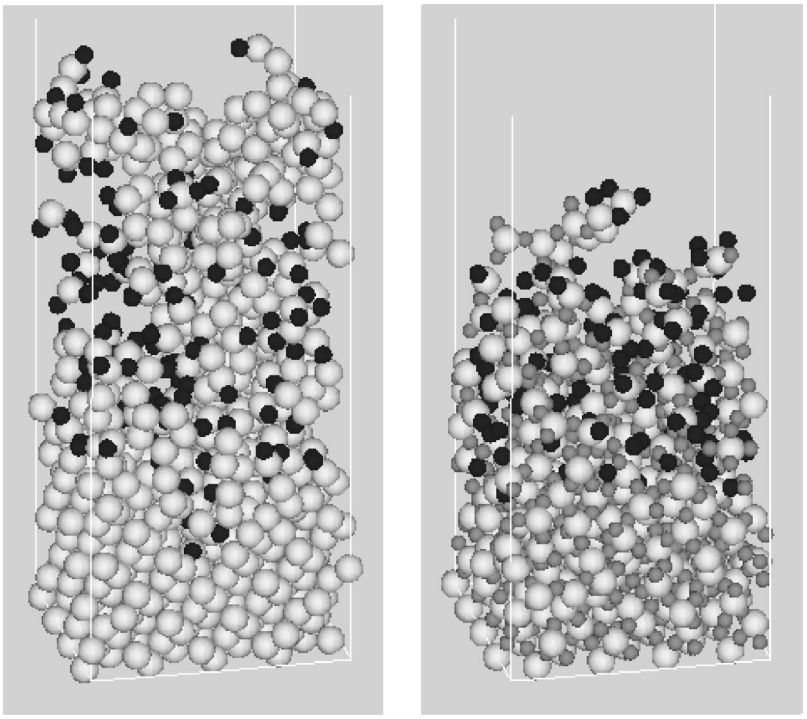

FIG. 5. Typical surface structures during 100 eV F beam etching; the Si (a) and SiO_2 (b) targets are shown. Large white spheres are Si atoms, small gray spheres are O atoms, and small black spheres are F atoms.

the oxide surface during Ar impact accounts for our observation that the sputtering threshold energies for Si and SiO_2 targets are almost the same (i.e., 45–47 eV). The threshold energy of Si sputtering from an oxide target is essentially determined by that from the pure Si surface since the Si concentration is significantly higher on the oxide surface than that in the bulk under Ar bombardment.

It is shown in Fig. 3 that the threshold energy of oxide etching by Cl impact is close to that by Ar sputtering. This is because oxide etching by Cl is almost pure physical sputtering in this energy regime. Figure 4 shows typical surface structures during 50 eV Cl beam etching. Figures 4(a) and 4(b) show Si and SiO_2 targets. It is seen that, at 50 eV impact energy, most of the Cl atoms stay on the top of the oxide target whereas a significant number of Cl atoms penetrate a few monolayers of the Si target. The difficulty for Cl atoms to penetrate the oxide may be caused by the facts (1) that the Si–O bond length is much smaller than the Si–Si bond length so that there is less room for Cl atoms to go through in the oxide target and (2) that the Si–O binding energy is much higher than the Si–Si binding energy. Therefore, at around 50 eV, impinging Cl atoms have only minor contributions to weakening Si–O bonds near the surface, resulting in little chemical enhancement for sputtering yields. As the Cl impact energy increases, however, Cl atoms penetrate the target more deeply and chemical enhancement of sputtering yields increases. For Si etching, however, the chemical enhancement of sputtering yields by Cl is much more significant than for SiO_2 etching and thus sputtering yields of Si are higher. This is because the Si–Cl binding energy is almost twice as large as the Si–Si binding energy, so that Cl atoms terminating Si bonds are stable in Si targets. On the other hand, the Si–Cl binding energy is slightly lower and the Cl–O binding energy is much lower than the Si–O binding energy, so that Cl atoms terminating Si bonds in SiO_2 targets are less stable. It follows that less energy is required to remove Si atoms by atomic bombardment from Si targets than from SiO_2 targets.

As in the case of Cl beam etching, F atoms also have more difficulty penetrating SiO_2 targets than Si targets. Figures 5(a) and 5(b) represent typical Si and SiO_2 surface structures during 100 eV F beam etching. It is seen that, at 100 eV impact energy, the thickness (i.e., depth) of the fluorinated layer is much larger for Si than that for SiO_2, which is also shown in Table III. Unlike Cl beam etching of oxide, the Si–F binding energy is higher than the Si–O energy, so that F atoms terminating Si bonds in oxide are somewhat more stable than Cl atoms in oxide. This stronger chemical effect of F may account for higher yields Y observed for F beam etching of oxide, as well as our observation that etching products contain more halogen atoms per Si atom for F beam etching than Cl beam etching with the same incident energy. The stoichiometry of etching products is shown in Fig. 6.

To represent silicon-oxide selectivities, we use the ratios of sputtering yields, rather than the ratios of etch rates. The ratios of sputtering yields are calculated from sputtering yield data in Table II and listed in Table IV. Here S denotes the ratio of Si sputtering yield of the Si target to that of the SiO_2 target with yield values taken from Y in Table II. Similarly, S_2 denotes the same ratio with yield values taken from Y_2 in Table II. Figure 7 plots yield ratio S for the three different cases: Cl (○), F (□), and Ar (△) beam etching. The fitting curves are obtained from the ratios of fitting curves

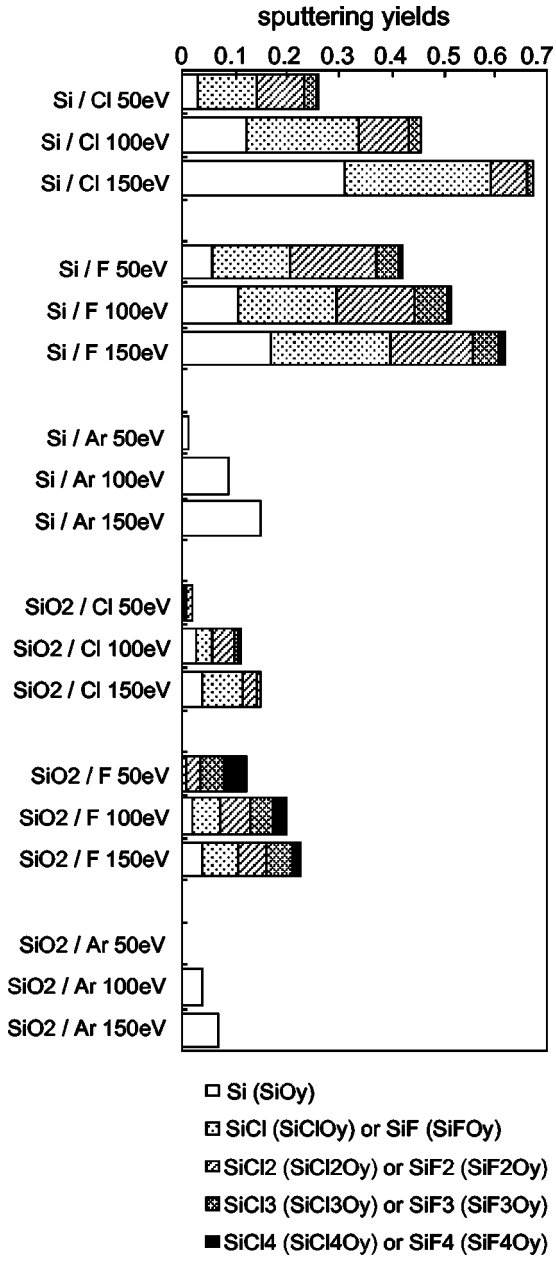

FIG. 6. Stoichiometry of etching products is shown. The horizontal axis represents the sputtering yield of each cluster (as denoted) that contains a single Si atom, i.e., the number of such clusters per incident atom.

TABLE IV. Silicon–oxide yield ratios S calculated from simulation data Y given in Table II are shown. Similarly S_2 are ratios calculated from Y_2 in Table II.

Beam	S	S_2
Cl 50 eV	13	13
Cl 100 eV	4.2	4.4
Cl 150 eV	4.5	4.0
F 50 eV	3.5	2.9
F 100 eV	2.6	2.4
F 150 eV	2.8	2.5
Ar 50 eV	3.5	3.5
Ar 100 eV	2.2	2.0
Ar 150 eV	2.2	1.7

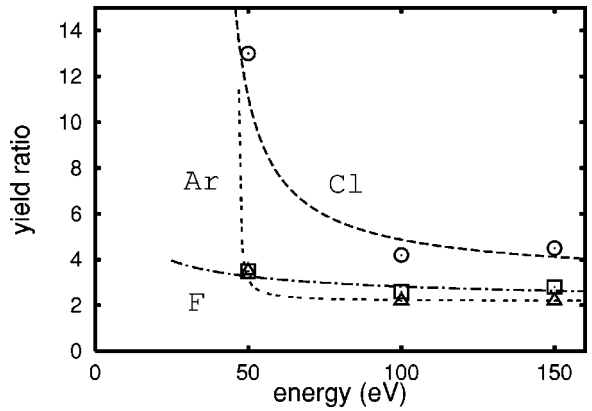

FIG. 7. Si–oxide yield ratios (S in Table IV) for Cl (○), F (□), and Ar (△) beam etching are shown. The dashed, dotted–dashed, and dotted curves are fitting curves for yield ratios in Cl, F, and Ar beam etching processes, respectively, which are the ratios of the corresponding yield fitting curves given in Figs. 2 and 3.

shown in Figs. 2 and 3. The results presented here are similar to the observations in RIE experiments by Oostra *et al.*[33]

In summary, we have performed MD simulations for silicon and silicon dioxide etching by energetic halogens (F, or Cl), using new sets of interatomic potentials representing Si–O–F and Si–O–Cl systems. Sputtering yields for silicon and oxide targets have been obtained from the MD simulations, which are in good agreement with experimental observations. Our MD simulations have also shown different target surface structures for fluorine and chlorine beam etching processes, which are essentially accounted for by the difference in atomic size and binding energy between fluorine and chlorine.

ACKNOWLEDGMENT

This work was supported in part by the 21st Century Kawasaki Foundation.

APPENDIX A

In this appendix, we present the potential functions that we used in the MD simulations. Following Stillinger and Weber,[1] we assume that the total potential energy of the system is given by

$$\Phi\sum_{i<j} v_2(i,j)+\sum_{i<j<k} v_3(i,j,k). \tag{A1}$$

Here, $v_2(i,j)$ is the pair-like interaction having the form

$$v_2(i,j)=g(i,j)A_{ij}(B_{ij}r_{ij}^{-p_{ij}}-r_{ij}^{-q_{ij}})\exp\left[\frac{C_{ij}}{r_{ij}-a_{ij}}\right] \quad \text{if } r_{ij}<a_{ij}, \tag{A2}$$

and $v_2(i,j)=0$, otherwise. By $r_{ij}=|\mathbf{r}_j-\mathbf{r}_i|$, we denote the distance between the i-th and j-th atoms located at $\mathbf{r}_i$ and $\mathbf{r}_j$. The parameters A_{ij}, B_{ij}, C_{ij}, p_{ij}, q_{ij}, and a_{ij} depend only on the element types of i-th and j-th atoms. The ''bond-

TABLE V. Parameters of the interatomic potential functions for Cl–O and F–O systems are shown.

Si–O–Cl			Si–O–F		
v_{ClO}	A_{ClO}	71.0	v_{FO}	A_{FO}	142.5
[Eq. (A2)]	B_{ClO}	0.471	[Eq. (A2)]	B_{FO}	0.2772
	C_{ClO}	3.55		C_{FO}	4.111
	p_{ClO}	3.13		p_{FO}	3.0
	q_{ClO}	1.53		q_{FO}	1.0
	a_{ClO}	1.8		a_{FO}	1.6
	R_{ClO}	1.0		R_{FO}	0.9
	D_{ClO}	0.1		D_{FO}	0.1
h_{ClClO}	λ_{ClClO}	1170	h_{FFO}	λ_{FFO}	1.135×10^{6}
[Eq. (A4)]	$\gamma^{\mathrm{Cl}}_{\mathrm{ClClO}}$	3.97	[Eq. (A4)]	$\gamma^{\mathrm{F}}_{\mathrm{FFO}}$	13.44
	$\gamma^{\mathrm{O}}_{\mathrm{ClClO}}$	3.24		$\gamma^{\mathrm{O}}_{\mathrm{FFO}}$	3.441
	$a^{\mathrm{Cl}}_{\mathrm{ClClO}}$	2.0862		$a^{\mathrm{F}}_{\mathrm{FFO}}$	2.0862
	$a^{\mathrm{O}}_{\mathrm{ClClO}}$	1.8		$d^{\mathrm{O}}_{\mathrm{FFO}}$	1.6
h_{ClOCl}	λ_{ClOCl}	78.3	h_{FOF}	λ_{FOF}	4720
[Eq. (A5)]	$\gamma^{\mathrm{Cl}}_{\mathrm{ClOCl}}$	1.83	[Eq. (A5)]	$\gamma^{\mathrm{F}}_{\mathrm{FOF}}$	3.608
	$a^{\mathrm{Cl}}_{\mathrm{ClOCl}}$	1.8		$a^{\mathrm{F}}_{\mathrm{FOF}}$	1.6
	$\cos\theta^{0}_{\mathrm{ClOCl}}$	−0.221		$\cos\theta^{0}_{\mathrm{FOF}}$	−0.048 24
	α_{ClOCl}	1.0		α_{FOF}	1.285
h_{OClO}	λ_{OClO}	1.66×10^{5}	h_{OFO}	λ_{OFO}	3.092×10^{4}
[Eq. (A4)]	$\gamma^{\mathrm{O}}_{\mathrm{OClO}}$	5.78	[Eq. (A4)]	$\gamma^{\mathrm{O}}_{\mathrm{OEO}}$	4.280
	$\alpha^{\mathrm{O}}_{\mathrm{OClO}}$	1.8		$\alpha^{\mathrm{O}}_{\mathrm{OFO}}$	1.6
h_{ClOO}[a]			h_{FOO}[b]		

[a] $h_{\mathrm{ClOO}}=0$.
[b] $h_{\mathrm{FOO}}=0$.

TABLE VI. Parameters of the three-body interatomic potential functions for Si–O–Cl (or F) systems are shown.

Si–O–Cl			Si–O–F		
h_{SiClO}	λ_{SiClO}	214	h_{SiFO}	λ_{SiFO}	1070
[Eq. (A4)]	$\gamma^{\mathrm{Si}}_{\mathrm{SiClO}}$	1.12	[Eq. (A4)]	$\gamma^{\mathrm{Si}}_{\mathrm{SiFO}}$	0.908
	$\gamma^{\mathrm{O}}_{\mathrm{SiClO}}$	3.24		$\gamma^{\mathrm{O}}_{\mathrm{SiFO}}$	4.45
	$\alpha^{\mathrm{Si}}_{\mathrm{SiClO}}$	1.8		$\alpha^{\mathrm{Si}}_{\mathrm{SiFO}}$	1.6
	$\alpha^{\mathrm{O}}_{\mathrm{SiClO}}$	1.8		$\alpha^{\mathrm{O}}_{\mathrm{SiFO}}$	1.6
h_{ClSiO}	λ_{ClSiO}	33.5	h_{FSiO}	λ_{FSiO}	3.13
[Eq. (A5)]	$\gamma^{\mathrm{Cl}}_{\mathrm{ClSiO}}$	0.295	[Eq. (A5)]	$\gamma^{\mathrm{F}}_{\mathrm{FSiO}}$	0.424
	$\gamma^{\mathrm{O}}_{\mathrm{ClSiO}}$	1.63		$\gamma^{\mathrm{O}}_{\mathrm{FSiO}}$	1.22
	$\alpha^{\mathrm{Cl}}_{\mathrm{ClSiO}}$	1.4		$\alpha^{\mathrm{F}}_{\mathrm{FSiO}}$	1.4
	$\alpha^{\mathrm{O}}_{\mathrm{ClSiO}}$	1.4		$\alpha^{\mathrm{O}}_{\mathrm{FSiO}}$	1.4
	$\cos\theta^{0}_{\mathrm{ClSiO}}$	0.0575		$\cos\theta^{0}_{\mathrm{FSiO}}$	0.396
	α_{ClSiO}	2.31		α_{FSiO}	3.15
h_{SiOCl}	λ_{SiOCl}	10.3	h_{SiOF}	λ_{SiOF}	47.8
[Eq. (A5)]	$\gamma^{\mathrm{Si}}_{\mathrm{SiOCl}}$	0.723	[Eq. (A5)]	$\gamma^{\mathrm{Si}}_{\mathrm{SiOF}}$	0.653
	$\gamma^{\mathrm{Cl}}_{\mathrm{SiOCl}}$	0.564		$\gamma^{\mathrm{F}}_{\mathrm{SiOF}}$	1.56
	$\alpha^{\mathrm{Si}}_{\mathrm{SiOCl}}$	1.4		$\alpha^{\mathrm{Si}}_{\mathrm{SiOF}}$	1.4
	$\alpha^{\mathrm{Cl}}_{\mathrm{SiOCl}}$	1.4		$\alpha^{\mathrm{F}}_{\mathrm{SiOF}}$	1.4
	$\cos\theta^{0}_{\mathrm{SiOCl}}$	−0.438		$\cos\theta^{0}_{\mathrm{SiOF}}$	−0.263
	α_{SiOCl}	1.05		α_{SiOF}	1.18

softening function'' $g(i,j)$ is assumed to be the same as that introduced by Watanabe *et al.*[22] for all oxygen–nonoxygen pairs.

The three-body term $v_3(i,j,k)$ in Eq. (A1) may be written as

$$v_3(i,j,k)=h_{jik}(r_{ij},r_{ik},\theta_{jik})+h_{ijk}(r_{ji},r_{jk},\theta_{ijk}) + h_{ikj}(r_{ki},r_{kj},\theta_{ikj}), \tag{A3}$$

with θ_{jik} being the angle spanned by vectors $\mathbf{r}_{ij}\equiv\mathbf{r}_j-\mathbf{r}_i$ and $\mathbf{r}_{ik}\equiv\mathbf{r}_k-\mathbf{r}_i$ at vertex $\mathbf{r}_i$. To construct interatomic potentials for Si–O–F (or Cl) systems, we employ the functional form[1] for h_{jik} given by either

$$h_{jik}(r,s,\theta)=\lambda_{jik}\exp\left[\frac{\gamma^{j}_{jik}}{r-a^{j}_{jik}}+\frac{\gamma^{k}_{jik}}{s-a^{i}_{jik}}\right], \tag{A4}$$

or

$$h_{jik}(r,s,\theta)=\lambda_{jik}\exp\left[\frac{\gamma^{j}_{jik}}{r-a^{j}_{jik}}+\frac{\gamma^{k}_{jik}}{s-a^{k}_{jik}}\right] \times|\cos\theta-\cos\theta^{0}_{jik}|^{2\alpha_{jik}}, \tag{A5}$$

depending on species of the ith atom if $r<a^{j}_{jik}$ and $s<a^{k}_{jik}$. Otherwise, $h_{jik}=0$. Here, λ_{jik}, γ^{j}_{jik}, γ^{k}_{jik}, α^{j}_{jik}, α^{k}_{jik}, θ^{0}_{jik}, and α_{jik} are parameters that depends on the species of (i, j, and k) triplet. We have modified the original SW function by introducing a new parameter α_{jik} in order to improve the parameter fitting.

The parameters in the Eqs. (A1)–(A5) for Si–F, Si–Cl, and Si–O systems are found in Refs. 1–5, and 22. We have determined the remaining parameters by fitting these equations to potential data obtained from *ab initio* calculations. The obtained parameters are listed in Tables V and VI. The employed energy and length units are 50.0 kcal/mol (2.17 eV) and 2.0951 Å. Details of the derivation of these parameters will be published elsewhere.[23]

[1] F. H. Stillinger and T. A. Weber, Phys. Rev. B **31**, 5262 (1985).
[2] F. H. Stillinger and T. A. Weber, J. Chem. Phys. **88**, 5123 (1988).
[3] F. H. Stillinger and T. A. Weber, Phys. Rev. Lett. **62**, 2144 (1989).
[4] T. A. Weber and F. H. Stillinger, J. Chem. Phys. **92**, 6239 (1990).
[5] H. Feil, J. Dieleman, and B. J. Garrison, J. Appl. Phys. **74**, 1303 (1993).
[6] M. E. Barone and D. B. Graves, J. Appl. Phys. **77**, 1263 (1995).
[7] M. E. Barone and D. B. Graves, J. Appl. Phys. **78**, 6604 (1995).
[8] B. A. Helmer and D. B. Graves, J. Vac. Sci. Technol. A **15**, 2252 (1997).
[9] D. E. Hanson, A. F. Voter, and J. D. Kress, J. Appl. Phys. **82**, 3552 (1997).
[10] N. A. Kubota, D. J. Economou, and S. J. Plimpton, J. Appl. Phys. **83**, 4055 (1998).
[11] B. A. Helmer and D. B. Graves, J. Vac. Sci. Technol. A **16**, 3502 (1998).
[12] B. A. Helmer and D. B. Graves, J. Vac. Sci. Technol. A **17**, 2759 (1999).
[13] P. C. Weakliem, C. J. Wu, and E. A. Carter, Phys. Rev. Lett. **69**, 200 (1992).
[14] P. C. Weakliem and E. A. Carter, J. Chem. Phys. **98**, 737 (1993).
[15] L. E. Carter, S. Khodabandeh, P. C. Weakliem, and E. A. Carter, J. Chem. Phys. **100**, 2277 (1994).
[16] D. E. Hanson, A. F. Voter, and J. D. Kress, J. Chem. Phys. **110**, 5983 (1999).
[17] D. E. Hanson, A. F. Voter, and J. D. Kress, J. Vac. Sci. Technol. A **17**, 1510 (1999).
[18] C. F. Abrams and D. B. Graves, J. Vac. Sci. Technol. A **16**, 3006 (1998).
[19] A. Kubota and D. J. Economou, IEEE Trans. Plasma Sci. **27**, 106 (1999).
[20] A. Kubota and D. J. Economou, IEEE Trans. Plasma Sci. **27**, 1416 (1999).
[21] H. Ohta and S. Hamaguchi, Phys. Rev. Lett. **84**, 6026 (2000).
[22] T. Watanabe, H. Fujiwara, H. Noguchi, T. Hosino, and I. Ohdomari, Jpn. J. Appl. Phys., Part 2 **38**, 366 (1999).
[23] H. Ohta and S. Hamaguchi, J. Chem. Phys. (submitted).
[24] I. Torrens, *Interatomic Potentials* (Academic, New York, 1972).
[25] R. Smith and D. E. Harrison Jr., Comput. Phys. **3**, 68 (1989).
[26] H. J. C. Berendsen, J. P. M. Postma, W. F. van Gunsteren, A. DiNola, and J. R. Haak, J. Chem. Phys. **81**, 3684 (1984).
[27] C. Steinbrüchel, Appl. Phys. Lett. **55**, 1960 (1989).
[28] J. P. Chang and H. H. Sawin, J. Vac. Sci. Technol. A **15**, 610 (1997).
[29] W. M. Holber and J. Forster, *Proceedings of Symposium on Dry Process*,

Tokyo, 1989 (IEEJ, Technical Committee on Electron Devices, 1989), p. 9.
[30]J. P. Chang, J. C. Arnold, G. C. H. Zau, and H.-S. Shin, J. Vac. Sci. Technol. A **15**, 1853 (1997).
[31]S. Tachi and S. Okudaira, J. Vac. Sci. Technol. B **4**, 459 (1986).
[32]M. Seel and P. S. Bagus, Phys. Rev. B **28**, 2023 (1983).
[33]D. J. Oostra, R. P. van Ingen, A. Haring, A. E. de Vries, and G. N. A. van Veen, Appl. Phys. Lett. **50**, 1506 (1987).